

Intrinsic linewidth calculation in an argon X-ray laser based on the model of geometrically dependent gain coefficient

A. HARIRI*, S. SARIKHANI

Laser and Optics Research Department, Nuclear Science and Technology Research Institute,
North Kargar Avenue, P.O. Box 11365-8486, Tehran, Iran

*Corresponding author: akbar_hariri@yahoo.com

By introducing differential amplified spontaneous emission intensity, numerical calculations for both homogeneously and Doppler broadened lines, and using the reported experimental measurements of the amplified spontaneous emission intensity and linewidth, we managed to explain the linewidth behavior, and calculate the intrinsic linewidth due to Voigt-profile width in an argon X-ray laser operating at 440×10^{-3} torr argon pressure and current of 21 kA. For the calculation, the intensity rate equation, along with the model of geometrically dependent gain coefficient were applied. The calculated value of the intrinsic linewidth was found to be 55.67 mÅ, which is very close to the Doppler broadened line of 53.52 mÅ. That is, the collision broadening has a very small contribution to the light-matter interaction in argon X-ray lasers. Details of the procedure used for the calculation will be presented in this paper.

Keywords: Ar X-ray laser, intrinsic linewidth, ASE.

1. Introduction

After the first successful demonstration of electron-collision excitation of soft X-ray using Se-target in 1985 [1], significant amplification has been observed in $3p-3s$ transition in Ne-like ions [1–7] and $4d-4p$ transitions in Ni-like ions [8, 9]. The subject for solid targets was also extensively investigated theoretically and reviewed [10–13]. In this direction, the characterization of a laser system under the study was also considered as an important issue. In gas phase, an Ar X-ray laser operating at 46.9 nm wavelength [14] has particularly attracted the worldwide attention, as it has the potential to be commercially available to be used as a practical tool in any laser laboratory. For understanding the behavior of X-ray lasers, in general, many theoretical models and mathematical approaches have also been proposed to predict and explain the lasers output behaviors, their coherencies and gain coefficients. From the experimental point of view, two types of measurements, namely, the amplified spontaneous emission (ASE)

output intensity I^{ASE} extracted from a laser system and the linewidth $\Delta\lambda^{\text{ASE}}$ vs. excitation length z , are commonly considered. For data analysis for the first type of measurements, usually Linford equation, proposed in 1974 [15], is used to extract unsaturated gain coefficients. The proposed equation, in spite of many attempts that have been made for its improvement [12, 16], encounters disadvantages to be used for deducing small signal gains. For example, it does not explain all the experimental data points of the ASE intensity vs. z , in particular when the measured I^{ASE} approaches the saturation limit. The I^{ASE} formula predicts that at $z = 0$, it is always equal to zero, whereas it has been established experimentally that the ASE starts at a threshold length z_{th} which is not zero, even for optically pumped small-sized samples [17, 18]. Selection of different portions of the I^{ASE} vs. z profile gives different values of the small signal gain [17]. In fact, by neglecting some random parts of the profile for data analysis, some valuable information that can be obtained from an experiment is left to be useless.

Based on our measurements, further analytical and numerical calculations for gas lasers [19], we managed to introduce the model of geometrically dependent gain coefficient (GDGC) for explaining gain coefficients in gas lasers such as N_2 , and excimer lasers. In these studies it was confirmed that gain coefficients are dominantly determined by the geometry of the laser systems. Subsequently, the model was successfully applied for the ASE gain and linewidth behaviors in KrF lasers [20, 21]. The only requirement for applying the model is the availability of the I^{ASE} and $\Delta\lambda^{\text{ASE}}$ vs. medium amplification length l_{amp} which can be obtained through measurements. In this paper, we are presenting the results of applying the GDGC model to explain linewidth behavior in an Ar X-ray laser. Both homogeneously and Doppler broadened line shapes are used for the calculation and finally the intrinsic linewidth which is initiated at the threshold length z_{th} is calculated. For the approach, the numerical calculation is applied, where the analytical calculation is also used for supporting the physical meaning behind the results obtained by the numerical calculations.

2. Theoretical approach

We start with the intensity rate equation, and by considering the saturation effect we can write [22],

$$\frac{\partial I^{\nu}(z)}{\partial z} = \frac{g_0^{\nu}(z)I^{\nu}(z)}{\left[1 + I^{\nu}(z)/I_s^{\nu}\right]^{\mu}} + \frac{g_0^{\nu}(z)h\nu}{\sigma_{\text{stim}}^{\nu}\tau_{\text{sp}}\left[1 + I^{\nu}(z)/I_s^{\nu}\right]^{\mu}} \gamma(z) \quad (1)$$

where I^{ν} is the ASE intensity, g_0^{ν} is the unsaturated small signal gain at frequency ν , and I_s^{ν} is the saturation intensity; $\sigma_{\text{stim}}^{\nu}$ and τ_{sp} are stimulated emission cross-section and the spontaneous emission lifetime of the medium upper state level, respectively; $\gamma(z) = \Omega(z)/4\pi$ specifies the nature of the ASE propagation, where $\Omega(z)$ is the solid angle subtended from the exit face of the medium as seen from a plane located at the z -position. In a capillary discharge $\gamma(z) = (\pi d_{\text{amp}}^2/4)/(4\pi z^2)$ is applied for the numer-

ical calculation; d_{amp} is the discharge tube diameter. For the upper state population N_2 we let $N_2 \cong g_0^v/\sigma_{\text{stim}}^v$. Equation (1) for $\mu = 0, 1/2$ and 1 is solved numerically; $\mu = 0$ corresponds to the case when the effect of saturation is not considered [20]; $\mu = 1/2$ and 1 correspond to the homogeneously (H) and Doppler (D) broadened transitions, respectively. For the case when $\mu = 1/2$ is used for the numerical calculation, $I_s^{v_0, H}$ which refers to the saturation intensity at the v_0 frequency for the H-broadened line is used in the dominator of this equation [22]. The saturation length z_{sat} in this case is defined when $I^{v_0} = I^{v_0, H}$, where for the saturated gain coefficient it gives $g^{v_0} = g_0^{v_0}/\sqrt{2}$. For the $\mu = 1$ solution when $I^{v_0} = I^{v_0, H}$, the saturated small signal gain coefficient is $g^{v_0} = g_0^{v_0}/2$.

To obtain the analytical solution for $I^v(z)$, we let $\mu = 0$. In this case, the solution for $\mu = 0$ can be readily obtained [20],

$$I^v = \frac{\gamma(z_{\text{th}})h\nu}{\sigma_{\text{stim}}^v \tau_{\text{sp}}} \left\{ \exp \left[\Delta G_0^v(z, z_{\text{th}}) \right] - 1 \right\} \quad (2)$$

where to solve the equation, the term $\gamma(z_{\text{th}})$, which is a constant and very close to the value obtained by the numerical calculation, is used; $\Delta G_0^v(z, z_{\text{th}}) = G_0^v(z) - G_0^v(z_{\text{th}})$ is defined. Also, $G_0^v(z) = \int g_0^v(z) dz$. In the GDGC model, it is proved that small signal gain at the central frequency v_0 is calculated to be [19]

$$g_0^{v_0}(z) = m' + \frac{1 + \gamma_L^{\text{max}}}{z} + b \gamma_L^{\text{max}} \sum_{n=1}^{\infty} \frac{n}{(n+1)!} (-bz)^n \quad (3)$$

where m' , γ_L^{max} and b are constants and they refer to gain parameters; γ_L^{max} is the maximum power losses. The saturation intensity at frequency v is given by [22, 23]

$$I_s^v = \frac{h\nu}{\sigma_{\text{stim}}^v \tau_u} = \frac{h\nu}{\sigma_{\text{stim}}^v \tau_{\text{sp}} \varphi} \quad (4)$$

where $\varphi = \tau_u/\tau_{\text{sp}}$ is the fluorescence quantum yield; τ_u is the medium upper state lifetime. By the use of Eq. (4), $I^v(z)$ in Eq. (2) simplifies to

$$I^v(z) = \gamma(z_{\text{th}}) I_s^v \varphi \left\{ \exp \left[\Delta G_0^v(z, z_{\text{th}}) \right] - 1 \right\} \quad (5)$$

Equation (5) shows that $I^v(z)$ is frequency dependent. We may also show this dependence explicitly. For the H- and D-broadened lines we have [23]:

$$\sigma_{\text{stim}}^{v, H} = \sigma_{\text{stim}}^{v_0, H} / (1 + x^2)$$

$$g_0^{v, H}(z) = g_0^{v_0, H}(z) / (1 + x^2)$$

$$I_s^{v, H} = (1 + x^2) I_s^{v_0, H}$$

also

$$\sigma_{\text{stim}}^{v, D} = \sigma_{\text{stim}}^{v_0, D} \exp(-x^2 \ln 2)$$

$$g_0^{v, D}(z) = g_0^{v_0, D}(z) \exp(-x^2 \ln 2)$$

$$I_s^{v, D} = I_s^{v_0, D} \exp(x^2 \ln 2)$$

then $\Delta G_0^v(z, z_{\text{th}})$ in Equation (5) will be $\Delta G_0^{v_0, H}(z, z_{\text{th}})/(1+x^2)$ and $\Delta G_0^{v_0, H}(z, z_{\text{th}}) \times \exp(-x^2 \ln 2)$, respectively, where superscripts H and D refer to H- and D-broadened lines. By substituting these last two expressions along with the $I_s^{v, H}$ and $I_s^{v, D}$ expressions shown in the above identities into Eq. (5), the ASE intensities with respect to x are obtained. The normalized frequency offset x for the H- and D-broadened lines is given by $x = 2(v - v_0)/\Delta v_0^H$ and $x = 2(v - v_0)/\Delta v_0^D$, respectively; Δv_0^H and Δv_0^D are their corresponding spontaneous emission linewidths [22, 23]. When the ASE starts at the threshold length z_{th} and propagates along the z -direction, it means that it is possible to measure the ASE intensity and linewidth with respect to excitation length z and this is always accomplished in any laser laboratory. By applying Eq. (3) into Eq. (1) and solving this equation numerically for $v = v_0$, gain parameters (m' , γ_L^{max} and b) for the central transition frequency v_0 can be deduced for a given ASE intensity measurement. For the linewidth calculation, it is also required to solve Eq. (1) numerically. In this case for both H- and D-lines we let $g_0^{v, H}(z) = g_0^{v_0, H}(z)/(1+x^2)$ and $g_0^{v, D}(z) = g_0^{v_0, D}(z) \exp(-x^2 \ln 2)$ in Eq. (1). Then, x is considered to be a parameter. By varying x we can also obtain the x -dependence of the ASE intensity at any given z_j . The FWHMs deduced from the profiles (for both H- and D-broadenings) will give the calculated ASE linewidths at z_j for both line broadenings. Subsequently $\Delta \lambda^{\text{ASE}, V}$, corresponding to Voigt integral for both lines, is obtained using the following expression [24]

$$\Delta \lambda^{\text{ASE}, V} = 0.5346 \Delta \lambda^{\text{ASE}, H} + \sqrt{0.2166 (\Delta \lambda^{\text{ASE}, H})^2 + (\Delta \lambda^{\text{ASE}, D})^2} \quad (6)$$

By extending the calculation for all z_j , our requirement for deducing the $\Delta \lambda^{\text{ASE}}$ vs. z profile is obtained.

If we consider the analytical calculation, Eq. (5) is used for $\mu = 0$. For this approach, we have already obtained

$$\Delta v^{\text{ASE}, H} / \Delta v_0^H = \sqrt{\ln 2 / \Delta G_0^{v_0, H}(z, z_{\text{th}})}$$

$$\Delta v^{\text{ASE}, D} / \Delta v_0^D = 1 / \sqrt{\Delta G_0^{v_0, D}(z, z_{\text{th}})}$$

for the H- and D-lines, respectively [18]. These last two expressions for the linewidths indicate that at z_{th} , we have nonfinite values for $\Delta \lambda^{\text{ASE}}$, as $\Delta G_0^{v_0}(z, z_{\text{th}}) \rightarrow 0$ for both broadenings. This definitely introduces an ambiguity also for the numerical calculations when Eq. (1) is used. For $x^2 \gg 1$, or very small z , however, we may consider cal-

culating the $I^V(z)$ -profile according to Eq. (5) and applying the $x^2 \gg 1$ limit. For the H- and D-broadened lines, respectively, we obtain

$$I^{v, H}(z) \cong I_{x \rightarrow \infty}^{v_0, H}(z) + \frac{1}{2} \frac{\Delta G_0^{v_0, H}(z, z_{th})}{1 + x^2} I_{x \rightarrow \infty}^{v_0, H}(z) \quad (7a)$$

$$I^{v, D}(z) \cong I_{x \rightarrow \infty}^{v_0, D}(z) + \frac{1}{2} \Delta G_0^{v_0, D}(z, z_{th}) \exp(-x^2 \ln 2) I_{x \rightarrow \infty}^{v_0, D}(z) \quad (7b)$$

where

$$I_{x \rightarrow \infty}^{v_0, H}(z) = \gamma(z_{th}) I_s^{v_0, H} \varphi \Delta G_0^{v_0, H}(z, z_{th})$$

$$I_{x \rightarrow \infty}^{v_0, D}(z) = \gamma(z_{th}) I_s^{v_0, D} \varphi \Delta G_0^{v_0, D}(z, z_{th})$$

are defined, and for a given z they are constants. It is understood from Eqs. (7a) and (7b) that by introducing the differential ASE intensities, defined by

$$\Delta I^{v, H}(z) = I^{v, H}(z) - I_{x \rightarrow \infty}^{v_0, H}(z)$$

$$\Delta I^{v, D}(z) = I^{v, D}(z) - I_{x \rightarrow \infty}^{v_0, D}(z)$$

we obtain pure Lorentzian and Gaussian frequency distributions for the H- and D-lines, respectively. This means that for $x^2 \gg 1$ the ASE linewidths are calculated to be, respectively, $\Delta v^{ASE, H} = \Delta v_0^H$ and $\Delta v^{ASE, D} = \Delta v_0^D$, *i.e.*, by eliminating the ASE intensity background, given by $I_{x \rightarrow \infty}^{v_0}$ for both lines, the ambiguities for nonfinite values for Δv^{ASE} at $z = z_{th}$ are removed and the H- and D-broadened spontaneous emission linewidths are obtained. This ambiguity exists for the linewidth calculations when $I^V(z)$ is used, and naturally it is impossible to obtain the exact value for the intrinsic linewidth as long as ΔI^V is not used. It is to be cited that the corresponding line-profiles for using $I^V(z)$ and $\Delta I^V(z)$ overlap at large z , while when $z \rightarrow z_{th}$ they tend to deviate from each other so that the latter one at $z = z_{th}$ gives a finite value for $\Delta \lambda^{ASE}$. For the numerical calculation, $x = 4$ is enough for calculating the intensity background $I_{x \rightarrow \infty}^{v_0}(z)$.

3. Results

For our study we use the results of measurements presented in [25]. The excitation range in this report is $l_{amp} = 18$ to 36 cm and Ar gas pressure is 440×10^{-3} torr. The peak amplitude of the current pulse is 21 kA. The contributions of the Lorentzian and Doppler line shapes are $\Delta \lambda_0^H = 3.96$ mÅ and $\Delta \lambda_0^D = 53.52$ mÅ, where they correspond to 5.4×10^{10} and 7.3×10^{11} Hz, respectively; and

$$\sigma_{stim}^{v_0, H} = \mathcal{G}^{v_0, H} (\lambda_0^2 / (8\pi n^2 \tau_{sp}))$$

where $\mathcal{G}^{v_0, H} = 2/(\pi\Delta v_0^H)$, and

$$\sigma_{\text{stim}}^{v_0, D} = \mathcal{G}^{v_0, D}(\lambda_0^2/(8\pi n^2\tau_{\text{sp}}))$$

where $\mathcal{G}^{v_0, D} = 2\sqrt{\ln 2/\pi}/\Delta v_0^D$ [12], and n is the medium index of refraction ($n = 1$). By calculating $\sigma_{\text{stim}}^{v_0, H}\tau_{\text{sp}} = 1.03 \times 10^{-23} \text{ cm}^2\text{s}$ and $\sigma_{\text{stim}}^{v_0, D}\tau_{\text{sp}} = 1.12 \times 10^{-24} \text{ cm}^2\text{s}$, and by the use of $\varphi = 0.05$, the saturation intensities are $I_s^{v_0, H} = 0.82 \times 10^7 \text{ W/cm}^2$ and $I_s^{v_0, D} = 7.53 \times 10^7 \text{ W/cm}^2$. It is seen that $I_s^{v_0, D} = 9.2 I_s^H$.

In [25] the measured ASE intensity is given in an arbitrary unit. In this calculation, however, based on the values of the saturation intensities $I_s^{v_0, H}$ and $I_s^{v_0, D}$, the intensity units are modified and are given in W/cm^2 . Thus, for the $I^v(z)$ calculation, when $\mu = 1$ and $\mu = 1/2$ are used, two sets of gain parameters, corresponding to the H- and D-broadened lines, are obtained. In Figure 1a the calculated I^{v_0} vs. l_{amp} for the H-broadened

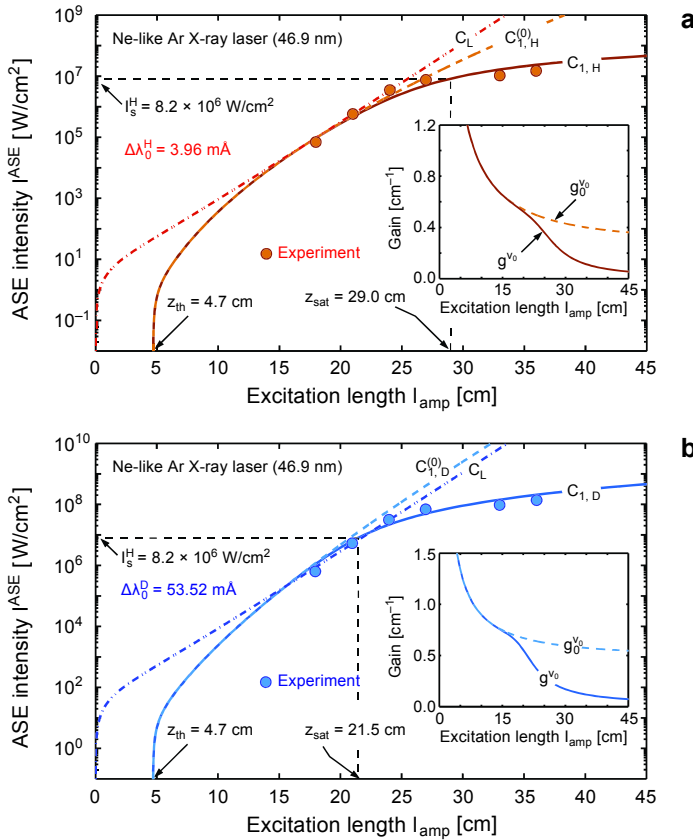


Fig. 1. Calculated results for the Ar X-ray laser output intensity vs. capillary discharge excitation length l_{amp} , for the H-broadened line (a) and D-broadened line (b). The $C_{1, H}$ - and $C_{1, H}^{(0)}$ -profiles refer to saturated and unsaturated calculations and the C_L -profile shows the fitting to Linford equation. Inset is the unsaturated $g_0^{v_0}$ and saturated $g_0^{v_0}$ gain profiles. Linford equation for both (a) and (b) figures gives $g_0^{v_0} = 0.62 \text{ cm}^{-1}$. Experimental measurements adopted from [25].

line is given. The $C_{1,H}$ -profile refers to the solution of Eq. (1) when $\mu = 1$ is used, while the $C_{1,H}^{(0)}$ -profile in this calculation refers to the case when $\mu = 0$ is applied, but gain parameters are used for the $\mu = 1$ solution. Thus, the $C_{1,H}$ - and $C_{1,H}^{(0)}$ -profiles refer to the saturated and unsaturated intensity solutions, respectively. The C_L -profile shows the results of the fitting to the experimental intensity measurements when the Linford equation is used, where it gives $g_0^{y_0} = 0.62 \text{ cm}^{-1}$. Significant differences between the $C_{1,H}$ - and C_L -profiles can be seen in this figure. In the inset of the figure, the unsaturated and saturated gain profiles are also given. For the excitation length of $l_{\text{amp}} = 36 \text{ cm}$, these profiles give $g_{0,H}^{y_0} = 0.38 \text{ cm}^{-1}$ and $g_{0,H}^{v_0} = 0.10 \text{ cm}^{-1}$. The threshold length is $z_{\text{th}} = 4.7 \text{ cm}$, and the saturation length is calculated to be $z_{\text{sat}} = 29.0 \text{ cm}$ (slightly higher than $z_{\text{sat}} \sim 24 \text{ cm}$, reported in [25]). Figure 1b shows the analysis made for the D-broadened line, where in this case $g_{0,D}^{y_0} = 0.57 \text{ cm}^{-1}$ and $g_{0,D}^{v_0} = 0.11 \text{ cm}^{-1}$ for $l_{\text{amp}} = 36 \text{ cm}$ are obtained. For the D-broadened line, $z_{\text{sat}} = 21.5 \text{ cm}$ is calculated, and is slightly different from that obtained in Fig. 1a for the H-broadened line. It is to be cited that while the $C_{1,H}$ - and $C_{1,D}$ -profiles explain the I^{ASE} measurements, the $C_{1,H}^{(0)}$ - and $C_{1,D}^{(0)}$ -profiles, corresponding to the unsaturated solutions, do not explain the ASE behavior and

Table. Calculated gain parameters, unsaturated and saturated gain coefficients for H- and D-lines, based on the reported measurements [25]; $l_{\text{amp}} = 36 \text{ cm}$, $d_{\text{amp}} = 300 \mu\text{m}$, and $p = 440 \times 10^{-3} \text{ torr}$; $b = 0.05 \text{ cm}^{-1}$ are used for the calculations. Errors are due to the method used for the calculation.

| Type of broadening | m' [cm^{-1}] | γ_L^{max} | $g_0^{y_0}$ [cm^{-1}] | g^{v_0} [cm^{-1}] |
|--------------------|---------------------------|-------------------------|----------------------------------|--------------------------------|
| H | 0.28 ± 0.04 | 5.50 ± 0.60 | 0.38 ± 0.03 | 0.10 ± 0.00 |
| D | 0.50 ± 0.04 | 3.30 ± 0.50 | 0.57 ± 0.03 | 0.11 ± 0.00 |

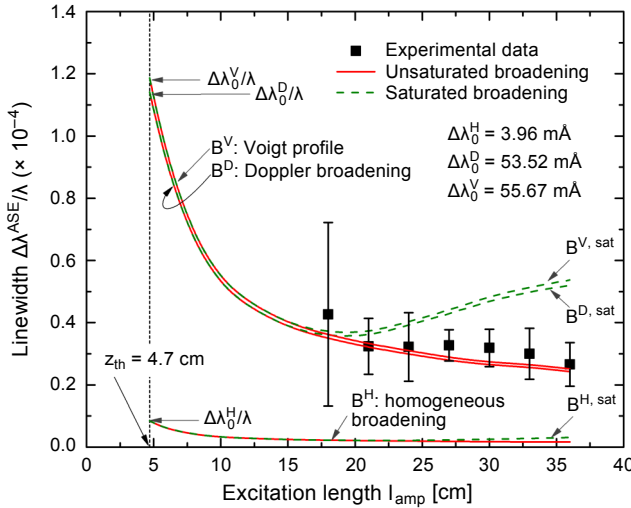


Fig. 2. The calculated ASE linewidth $\Delta\lambda^{\text{ASE}}/\lambda$ with respect to excitation length l_{amp} for the H- and D-broadened line shapes. The Voigt profile (B^V -profile) is calculated to be very close to the inhomogeneously broadened line (B^D -profile). The dashed profiles ($B^{H,\text{sat}}$ and $B^{D,\text{sat}}$) show the re-broadening and have no contribution to the broadening mechanisms.

they give profiles close to those predicted by the Linford equation. We also notice from these figures that the Linford equation always gives zero values for the ASE intensities when $z = 0$. In the Table a summary of the calculated results is given. The most elegant observation in this study for applying the GDGC model is the linewidth calculation shown in Figs. 2 and 3. For the calculations, the gain parameters are as those obtained from Fig. 1. It is seen in Fig. 2 that the H-broadened line (when $\mu = 1$) has a small contribution to the broadening mechanism (the B^H -profile), while the B^D -profile corresponding to the $\mu = 1/2$ solution, can explain the measurements. Consequently, the contribution of the Voigt-profile (the B^V -profile) corresponding to the H- and D-broadenings can be also visualized in this figure. In fact the B^D - and B^V -profiles in this study are very close to each other and they both, with a small difference can explain the measurements. The B^H - and B^D -profiles corresponding to the $C_{1,H}^{(0)}$ - and $C_{1,D}^{(0)}$ -calculated profiles (unsaturated), are shown in Fig. 1. The GDGC model also predicts the re-broadening linewidth, as shown by the B^{sat} -profiles in Fig. 2. These linewidths behavior are obtained by using gain parameters from Fig. 1 using $\mu = 1$ and $\mu = 1/2$ solutions, with the gain parameters obtained from the Table ($C_{1,H}$ and $C_{1,D}$ -profiles). For $z < 15$ cm the re-broadening effects for two lines disappear. According to the experimental linewidth measurements, however, these re-broadening effects have not been observed and therefore should not be further considered. One particular aspect of the linewidth calculation is the linewidth behavior near z_{th} . According to our previously introduced method to obtain a finite value for the linewidth at z_{th} , the FWHM of the $\Delta I^V(z)$ -profile, instead of the $I^V(z)$ -profile, has to be evaluated. The calculated results corresponding to this computation is given in Fig. 3. The C_1 -profile (solid line) in this

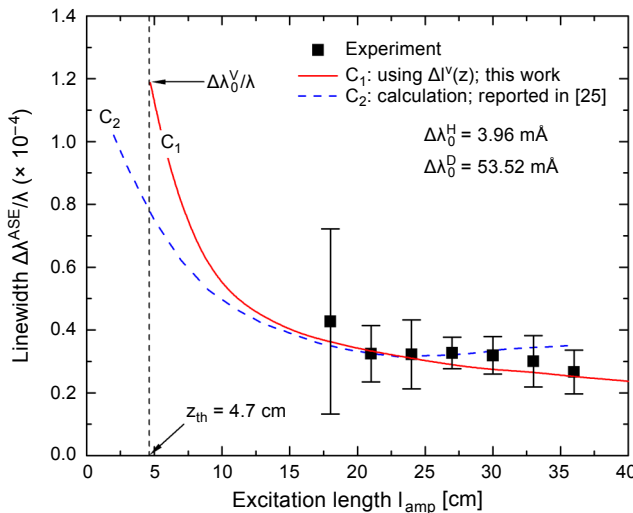


Fig. 3. The calculated linewidth $\Delta\lambda^{ASE}/\lambda$ vs. l_{amp} for using $\Delta I^V(l_{amp})$ for the FWHM calculations (C_1 -profile). For $z \rightarrow z_{th}$ the C_1 -profile gives the intrinsic linewidth of 55.67 mÅ. The C_2 -profile is the calculated linewidth as presented in [25], to be compared with the calculation made in this work. Experimental measurements were adopted from [25].

figure corresponds to the $\Delta\lambda^{\text{ASE, V}}/\lambda$, where $\Delta\lambda_0^{\text{H}} = 3.96 \text{ m\AA}$ and $\Delta\lambda_0^{\text{D}} = 53.52 \text{ m\AA}$ are used for the calculation. In this figure, our linewidth calculation is also compared with that presented in [25], shown by the C_2 -profile (dashed line). In the related calculations reported in [25] where the ion-ion collisions introduced in [26] and the molecular dynamics computation [27] were used, a slightly higher re-broadening is predicted, showing a small deviation from the measurements, and definitely their method does not predict the value of the intrinsic linewidth that occurs at z_{th} . Thus, with the introduced method of calculation for the linewidth, it can be concluded that:

1. The D-broadened line has the major responsibility for the broadening mechanism in a low pressure Ar X-ray laser.
2. The re-broadening mechanism (shown by dashed lines in Fig. 2) does not contribute to the light-matter interaction in the Ne-like Ar X-ray laser.
3. The theoretical approach explains measurements correctly with the intrinsic linewidth of $\Delta\lambda_0^{\text{V}} = 55.67 \text{ m\AA}$ which is very close to the Doppler linewidth of $\Delta\lambda_0^{\text{D}} = 53.52 \text{ m\AA}$.
4. The calculations, based on the GDGC model, show a gradual decrease in the linewidth when l_{amp} increases.

4. Conclusion and discussion

Using the model of geometrically dependent gain coefficient (GDGC), and experimental results of the ASE intensity and linewidth vs. capillary discharge length of an Ar X-ray laser, a calculation was carried out for both H- and D-broadening lines to obtain the intrinsic linewidth. It was found that the linewidth with respect to l_{amp} is dominantly determined by Doppler broadening mechanism, and collision broadening has a small contribution to the broadening mechanism. In the numerical calculation, in contrast to using the ASE intensity alone, *i.e.*, $I^{\text{ASE}}(z)$, it was realized that z -dependent values of the ASE intensity background must be subtracted from the $I^{\text{ASE}}(z)$ -profile to obtain $\Delta I^{\text{ASE}}(z)$. With this approach we reached a finite value for the linewidth at the threshold length z_{th} . The numerical calculation is also supported by the analytical approach, where it resulted in $\Delta\lambda^{\text{ASE, V}} = 55.67 \text{ m\AA}$. As $z_{\text{th}} = 4.7 \text{ cm}$ is large enough, so, letting the $z_{\text{th}} \rightarrow 0$ condition, which is a common method for small-sized samples [10], cannot be used. It deserves mentioning that the predictions that can be made using the GDGC model should not be compared with the reported results of the calculations using different mathematical approaches. The GDGC model not only simplifies the method of the calculation, but also, it relies on an excellent agreement with the experimental measurements. For example, the presence of the threshold length z_{th} where it is the ASE start point, although it has been introduced in the earliest reported theoretical investigations presented in [28], it has not been further considered in the related ASE solutions reported in the literature. Thus, by neglecting this parameter, a great amount of information is lost naturally. Also, for using the GDGC model, it is necessary to solve the intensity rate equation for both lines separately and then the corresponding Voigt-profile should be calculated. By observing and comparing the results of calculations with

the measurements, one can finalize the conclusion. In fact, the GDGC model, as shown in [29], is based on introducing the geometrical loss, where it leads to correct prediction for the light matter interaction.

References

- [1] MATTHEWS D.L., HAGELSTEIN P.L., ROSEN M.D., ECKART M.J., CEGLIO N.M., HAZI A.U., MEDECKI H., MACGOWAN B.J., TREBES J.E., WHITTEN B.L., CAMPBELL E.M., HATCHER C.W., HAWRYLUK A.M., KAUFFMAN R.L., PLEASANCE L.D., RAMBACH G., SCOFIELD J.H., STONE G., WEAVER T.A., *Demonstration of a soft X-ray amplifier*, Physical Review Letters **54**(2), 1985, pp. 110–113.
- [2] ROSEN M.D., HAGELSTEIN P.L., MATTHEWS D.L., CAMPBELL E.M., HAZI A.U., WHITTEN B.L., MACGOWAN B., TURNER R.E., LEE R.W., CHARATIS G., GAR. E. BUSCH, SHEPARD C.L., ROCKETT P.D., *Exploding-foil technique for achieving a soft X-ray laser*, Physical Review Letters **54**(2), 1985, pp. 106–109.
- [3] CAIRNS G.F., HEALY S.B., LEWIS C.L.S., PERT G.J., ROBERTSON E., *A time-resolved spectroscopy study of the resonance-line emission in the Ge XXIII XUV laser*, Journal of Physics B: Atomic, Molecular and Optical Physics **29**(20), 1996, pp. 4839–4854.
- [4] ALESSI D., LUTHER B.M., WANG Y., LAROTONDA M.A., BERRILL M., ROCCA J.J., *High repetition rate operation of saturated tabletop soft X-ray lasers in transitions of neon-like ions near 30 nm*, Optics Express **13**(6), 2005, pp. 2093–2098.
- [5] GANG YUAN, KATO Y., MURAI K., DAIDO H., KODAMA R., *Measurement of linewidths of Ne-like germanium soft x-ray laser in slab targets*, Journal of Applied Physics **78**(6), 1995, pp. 3610–3616.
- [6] HEALY S.B., JANULEWICZ K.A., PLOWES J.A., PERT G.J., *Transient high gains at 196 Å produced by picosecond pulse heating of a preformed germanium plasma*, Optics Communications **132**(4–6), 1996, pp. 442–448.
- [7] CARILLON A., CHEN H.Z., DHEZ P., DWIVEDI L., JACOBY J., JAEGLE P., JAMELOT G., JIE ZHANG, KEY M.H., KIDD A., KLISNICK A., KODAMA R., KRISHNAN J., LEWIS C.L.S., NEELY D., NORREYS P., O’NEILL D., PERT G.J., RAMSDEN S.A., RAUCOURT J.P., TALLENTS G.J., UHOMOIBHI J., *Saturated and near-diffraction-limited operation of an XUV laser at 23.6 nm*, Physical Review Letters **68**(19), 1992, pp. 2917–2920.
- [8] DUNN J., LI Y., OSTERHELD A.L., NILSEN J., HUNTER J.R., SHLYAPTSEV V.N., *Gain saturation regime for laser-driven tabletop, transient Ni-like ion X-ray lasers*, Physical Review Letters **84**(21), 2000, pp. 4834–4837.
- [9] GUILBAUD O., KLISNICK A., JOYEUX D., BENREDJEM D., CASSOU K., KAZAMIAS S., ROS D., PHALIPPOU D., JAMELOT G., MÖLLER C., *Longitudinal coherence and spectral profile of a nickel-like silver transient soft X-ray laser*, The European Physical Journal D **40**(1), 2006, pp. 125–132.
- [10] KOCH J.A., MACGOWAN B.J., DA SILVA L.B., MATTHEWS D.L., UNDERWOOD J.H., BATSON P.J., LEE R.W., LONDON R.A., MROWKA S., *Experimental and theoretical investigation of neonlike selenium X-ray laser spectral linewidths and their variation with amplification*, Physical Review A **50**(2), 1994, pp. 1877–1898.
- [11] HOLDEN P.B., HEALY S.B., LIGHTBODY M.T.M., PERT G.J., PLOWES J.A., KINGSTON A.E., ROBERTSON E., LEWIS C.L.S., NEELY D., *A computational investigation of the neon-like germanium collisionally pumped laser*, Journal of Physics B: Atomic, Molecular and Optical Physics **27**(2), 1994, pp. 341–367.
- [12] TALLENTS G.J., *The physics of soft X-ray lasers pumped by electron collisions in laser plasmas*, Journal of Physics D: Applied Physics **36**(15), 2003, pp. R259–R276.
- [13] MACGOWAN B.J., DA SILVA L.B., FIELDS D.J., KEANE C.J., KOCH J.A., LONDON R.A., MATTHEWS D.L., MAXON S., MROWKA S., OSTERHELD A.L., SCOFIELD J.H., SHIMKAVEG G., TREBES J.E., WALLING R.S., *Short wavelength X-ray laser research at the Lawrence Livermore National Laboratory*, Physics of Fluids B: Plasma Physics **4**(7), 1992, pp. 2326–2337.

- [14] ROCCA J.J., *Table-top soft X-ray lasers*, Review of Scientific Instruments **70**(10), 1999, pp. 3799–3827.
- [15] LINFORD G.J., PERESSINI E.R., SOOY W.R., SPAETH M.L., *Very long lasers*, Applied Optics **13**(2), 1974, pp. 379–390.
- [16] PERT G.J., *Output characteristics of amplified-stimulated-emission lasers*, Journal of the Optical Society of America B **11**(8), 1994, pp. 1425–1435.
- [17] HARIRI A., SARIKHANI S., *Application of the geometrically dependent gain coefficient model to describe amplified spontaneous emission behavior in organic solid laser materials: theoretical considerations*, Journal of Modern Optics **62**(10), 2015, pp. 822–829.
- [18] HARIRI A., SARIKHANI S., *Study of spectral linewidth in Ne-like Se X-ray laser*, Applied Optics **54**(33), 2015, pp. 9681–9687.
- [19] HARIRI A., SARIKHANI S., *A two dimensional theoretical model for describing gain coefficient in N₂-lasers and the model validity for CVL and excimer lasers*, Optics Communications **284**(8), 2011, pp. 2153–2163.
- [20] HARIRI A., SARIKHANI S., *Theoretical application of z-dependent gain coefficient to describe amplified spontaneous emission*, Optics Letters **37**(6), 2012, pp. 1127–1129.
- [21] HARIRI A., SARIKHANI S., *Study of the amplified spontaneous emission spectral width and gain coefficient for a KrF laser in unsaturated and saturated conditions*, Laser Physics Letters **11**(1), 2014, article ID 015003.
- [22] YARIV A., *Quantum Electronics*, 3rd Ed., Jhon Wiley and Sons, New York, 1989.
- [23] SVELTO O., *Principles of Lasers*, 5th Ed., Springer, 2010.
- [24] OLIVERO J.J., LONGBOTHUM R.L., *Empirical fits to the Voigt line width: a brief review*, Journal of Quantitative Spectroscopy and Radiative Transfer **17**(2), 1977, pp. 233–236.
- [25] URBANSKI L., MARCONI M.C., MENG L.M., BERRILL M., GUILBAUD O., KLISNICK A., ROCCA J.J., *Spectral linewidth of a Ne-like Ar capillary discharge soft-X-ray laser and its dependence on amplification beyond gain saturation*, Physical Review A **85**(3), 2012, article ID 033837.
- [26] LEE Y.T., MORE R.M., *An electron conductivity model for dense plasmas*, Physics of Fluids **27**(5), 1984, pp. 1273–1286.
- [27] TALIN B., DUFOR E., CALISTI A., GIGOSOS M.A., GONZÁLEZ M.A., DEL RÍO GAZTELURRUTIA T., DUFTY J.W., *Molecular dynamics simulation for modelling plasma spectroscopy*, Journal of Physics A: Mathematical and Theoretical **36**(22), 2003, pp. 6049–6056.
- [28] ALLEN L., PETERS G.I., *Amplified spontaneous emission II. The connection with laser theory*, Journal of Physics A: General Physics **4**(3), 1971, pp. 377–381.
- [29] HARIRI A., SARIKHANI S., *Theoretical study of amplified spontaneous emission in Ne-like Se X-ray laser: spectral linewidth and gain coefficient*, Optical and Quantum Electronics **48**(3), 2016, article ID 214.

*Received August 22, 2016
in revised form September 21, 2016*